ELSEVIER

Thin Solid Films 342 (1999) 282–290

thin solid films

Aluminium oxide tunnel junctions: influence of preparation technique, sample geometry and oxide thickness

D. Diesing*, A.W. Hassel[1], M.M. Lohrengel

Institut für Physikalische Chemie und Elektrochemie, Institut für Physik der kondensierten Materie, Heinrich-Heine-Universität Düsseldorf, Universitätsstr. 1, D40225 Düsseldorf, Germany

Received 26 February 1998; accepted 11 September 1998

Abstract

Tunnel junctions of the type Al/Al oxide/Ag can emit hot electrons of about 2 eV to an adjacent electrolyte and cause redox reactions. We developed a production technique of such tunnel systems, which are stable at room temperature in atmosphere and in electrolyte. Two types of Al base electrodes (wires and evaporated films on glass), three types of oxide films (gas phase oxidation, anodic oxidation and physical vapour deposition) were combined with an Ag top electrode film of 15 nm thickness. PVD oxide films are porous with a large thickness distribution. This causes a rough silver top electrode and therefore a weak corrosion resistance. Stable oxide films were only obtained for the pairs Al wire/anodic oxide and Al film/gas phase oxide. The oxides are almost equal in their properties and form dense homogenous films independent of the sample geometry. Anodic films can be formed with various thicknesses, but ionic currents may exceed the tunnel currents. A successful layer sequence was Al film/gas phase oxide (2.5 nm)/Ag (15 nm) with an emission current of hot electrons of about 1 mA/cm^2.

Keywords: Aluminium oxide films; Tunnel junctions; Impedance spectroscopy; Transients

1. Introduction

Electrons can pass through thin insulating films by direct elastic tunnel processes. In systems of the type metal 1/ insulator/metal 2 the tunnel current depends exponentially on the potential difference ΔU between the two metals and on the inverse thickness of the insulator. The fundamentals of electron tunnelling through thin, insulating films were given by Simmons [1]. If the metal 2 is polarised positively, electrons tunnel to metal 2 at an energy of e0ΔU above the Fermi level in metal 2. The mean free path (*mfp*) of these hot electrons in metal 2 is limited by two processes: (1) hot electron Fermi electron interaction (e.g. $mfp = 30$ nm in Ag, $\Delta U = 1.5$ V [2], (2) hot electron phonon interaction; this process has a low scattering probability for these electrons [3]. Therefore a large fraction of the hot electrons can penetrate metal films of less than 20 nm thickness. At the outer interface of metal 2 these electrons can excite surface plasmon polaritons and emit their energy by photons [4,5] or the electrons cross the interface and can be detected outside [6,7]. The latter process opens a wide field of applications, such as tuneable light sources or low temperature electron sources. This electron source is not limited to an interface metal 2/vacuum, but can be used also in contact with an electrolyte.

Electrochemical processes are normally driven by the potential difference at the interface metal /electrolyte. This potential difference influences further parameters like surface concentration, adsorption, and orientation of products, educts and intermediates. By hot electrons chemical reactions can be stimulated at almost random potential differences to reveal reaction paths and kinetics. Further applications might be electrochemical redox sensors for the detection of oxidisable or reducable components in liquids or atmosphere.

Thereby tunnel junctions must be prepared, which produce sufficient numbers of hot electrons and withstand environmental attacks. Promising were junctions of the type aluminium/ aluminium oxide/silver with oxide thicknesses of 2–10 nm and silver electrodes of 15–20 nm.

Aluminium oxide films represent almost perfect insulators. A considerably high specific resistance (10^{13} Ω cm) is combined with an extremely small diffusion of oxygen or water (growth rate of oxide film is less than 10 pm/d). This is only true for low field strengths, at higher field strengths

* Corresponding author.
E-mail address: diesing@uni-duesseldorf.de (D. Diesing)
[1] Present address: Laboratory of Interfacial Electrochemistry, Graduate School of Engineering, Hokkaido University, Sapporo 0608628, Japan

0040-6090/99/$ - see front matter
PII: S0040-6090(98)01427-8

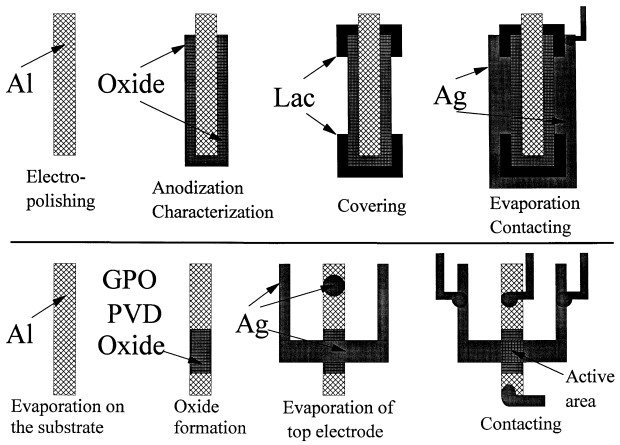

Fig. 1. Successive preparation steps of Al/oxide/Ag junctions on wires (cross-section, top) or on glass slides (top view, bottom).

($E > 1$ MV/cm, or potential differences of some 100 mV to some V, correspondingly) charge transport becomes possible, reducing the resistance of the film down to values of KΩ or Ω. Ion transport is a thermally activated hopping process, presumably a simultaneous migration of Al^{3+} and O^{2-} [8]. Due to the high concentration of mobile ions the space charges of anions and cations cause simultaneous migration with transport numbers close to 0.5 at higher field strengths [9]. This is valid in an electrochemical environment, in the case of a metal/oxide/metal system an oxygen support by the electrolyte is excluded. Ionic processes through the oxide barrier change the properties of the tunnel junctions and thus limit the lifetime of the sample.

A separation of electronic, ionic and tunnel currents is necessary to determine the efficiency of hot electron production and to characterise the junction. It becomes possible by comparison of samples of the type metal/aluminium oxide/metal and metal/aluminium oxide/electrolyte. This means that one electrode is varied from an exclusively electronic conductor to an exclusively ionic conductor.

The structure of the layers of a junction can be varied by the preparation techniques and can be influenced by the geometry of the sample. We investigated the systems Al/oxide/Ag (MIM), Al/oxide/electrolyte (MIE). The aluminium oxide films were formed by physical vapour deposition (PVD), gas phase oxidation with pure dry oxygen (GPO), and by anodic oxidation in an aqueous acetate buffer. Evaporated Al films or Al wires served as base electrodes.

Evaporated silver films of max. 20 nm thickness were used as top electrodes. The top electrodes must be as thin as possible to guarantee a predominant elastic transfer of the hot electrons. Monte Carlo simulations have shown that e.g. 15% of hot electrons (2 eV above Fermi level) cross elastically a 30 nm silver film [10]. On the other hand the top electrode must be thick enough to withstand corrosion attacks of the electrolyte (typically >15 nm).

Altogether, our aim was the preparation of homogeneous, dense oxide films with a well defined, variable film thickness, high breakdown stability, maximum electron efficiency, stability against corrosion, and long term stability.

2. Experimental

2.1. Chemical

Highly pure aluminium wires (99.999%) were used for the preparation of the wire type specimen. The same material was used as a source for the preparation of evaporated aluminium films. Solutions were prepared from p.a. chemicals and deionized water (Millipore Q). For the formation and investigation with electrolyte contact an acetate buffer of pH 6.0 was used. Physical vapour deposited oxide films were prepared from highly pressed aluminium oxide pellets (Balzers).

2.2. UHV chamber

The UHV Chamber was a Riber system with a turbo molecular pump, an ion getter, and a kryo pump. The base pressure was 1×10^{-6} Pa. During evaporation of aluminium or silver the pressure was held at 1×10^{-5} Pa. The thickness of the evaporated films was determined with a VEECO quartz crystal micro balance.

2.3. Electrochemical cell and electrolytes

The preparation of anodic oxide films and the electrochemical investigations were carried out in a Duran glass cell thermostatted to 25°C by a Haake D3 thermostat. A gold foil (4 cm^2) was used as a counter electrode. The reference electrode (Hg/Hg_2SO_4/1M Na_2SO_4) was connected in parallel with a gold wire and a 1 μF capacitor as a low resistance path. All potentials in the electrolyte given here refer to the hydrogen electrode in the same solution (HESS). The electrolyte was an acetate buffer (pH = 6.0, 74.2 g/dm^3 sodium acetate, 2.9 g dm^3 glacial acetic acid). To replace solved oxygen the buffer was de-purged with pure nitrogen (99.999%) for 10 min.

2.4. Electronic equipment

The electronic equipment consisted of a fast rising potentiostat (rise time < 300 ns), a pulse generator system for multiple pulses (-10 V $\leq U_{pulse} \leq 10$ V; 1 μs $\leq t_{pulse} \leq 10^6$ s), a fast autoranging current detection system (10 pA $\leq i \leq 2$ A; switching time $\leq$ 300 ns) and a transient recorder (two 12 bit analog to digital converters, sample frequency up to 1 MHz), all in-house developments.

2.5. Impedance spectroscopy

The conductivity (real and imaginary component) was determined by impedance measurements. Impedance spec-

tra were recorded in the range 10 mHz $\leq f \leq$ 10 MHz with an AC amplitude of 1 mV using a frequency response analyzer (Solartron Schlumberger 1255) combined with the electronic equipment described above. At frequencies lower than 100 mHz a switched capacity filter was used to minimise the noise.

3. Preparation

Fig. 1 shows the successive steps of the preparation of wire type and thin-film type junctions. A detailed description of the different subtypes is given in this chapter.

3.1. Metal substrate

3.1.1. Evaporated Films

Microscopic slides were used as an evaporation substrate. The slides were cleaned in an ultrasonic bath using first sulphuric acid and then ethanol.

3.1.1.1. Al:

The deposition rate of the aluminium base electrode was 200 pm/s and the final thickness of the Al film was 30 nm. Any time a new tungsten spiral was used for melting the aluminium to avoid a pollution of the evaporated aluminium films. The system was maintained during the deposition at a pressure of 1×10^{-5} Pa. If the pressure exceeds 1×10^{-4} Pa during aluminium deposition, parts of the base metal are oxidised. The quality of the aluminium films was proved by conductivity measurements [11].

3.1.1.2. Ag:

The silver top electrodes were deposited with a rate of 50 pm/s at a pressure of 5×10^{-5} Pa from a tantalum shell.

3.1.2. Wires

Aluminium wires with a diameter of 0.5 mm and a surface of about 0.3 cm^2 were used for the preparation of the wire specimen. The specimen were electropolished at a current density of 200 mA/cm^2 for 30 s in glacial acetic acid containing 5% perchloric acid. Specimen and solution were strongly stirred during electropolishing to avoid surface inhomogenities caused by the deposition of reaction products. After rinsing with Millipore water the specimen were immediately immersed into the electrolyte under potential control. An immersion potential of 0 V (HESS, hydrogen electrode in same solution) was used to avoid hydrogen evolution or further anodic oxide growth.

3.2. Oxide Films

A problem that arises if differently prepared oxide films are compared is the correct determination of the film thickness. According to the preparation process different methods were chosen. The oxide film thickness during evaporation was monitored by a quartz crystal micro balance (resolution 1 Hz).

During anodic oxidation in a non-corrosive electrolyte like acetate buffers side reactions can be neglected. Therefore the charge determined by numerical integration of the anodic current transients is only consumed by oxide formation. The film thickness was calculated from Faraday's law.

The thickness data from this coulometric method were compared with other methods like ellipsometry [12,13], electrochemical quartz crystal micro balance [14], angular resolved X-ray photoelectron spectroscopy (ARXPS) [13], sputter depth profile (argon sputtering 4 KeV) [15], transmission electron microscopy (TEM) [16].

3.2.1. Low temperature gas phase oxidation

After evaporation of the aluminium film in the UHV chamber (see Section 2.2), the recipient was flooded with pure oxygen (99.999%). The samples were exposed to the oxygen atmosphere for 2 h at room temperature. The resulting oxide thickness after this gas phase oxidation (GPO) was 2.5 nm (see Section 4.3.2)

3.2.2. Low temperature physical vapour deposition

For the evaporation of the aluminium oxide highly compressed pellets were used. The electron gun worked with a voltage of 4.2 KV. During the deposition the pressure within the chamber was better than 3×10^{-6} Pa to avoid pollution of the oxide film by electrical discharges within the chamber. The oxide film thickness from physical vapour deposition (PVD) determined by quartz crystal micro balance was about 10 nm. These values are only nominal since the structure of these films is very inhomogeneous. This will be discussed later.

3.2.3. Anodic oxidation

The probe was potentiostatted in the acetate buffer to 0 V (HESS) to remove a native film (air contact, about 2 nm) by the slow corrosion (250 fm/s [17]). After 1000 s the corrosion is stationary at an oxide thickness of 2.6 nm. Then the specimen was switched to the oxide formation potential $U_{form} > 0$ V for 1000 s. The resulting current transients were recorded with a time resolution of 1 μs. The charge was determined by numerical integration of the current. From such experiments a film formation factor of 1.6 nm/V was obtained, which is in good agreement with [18,19]. The high field strength during potentiostatic formation guarantees the formation of homogeneous, dense amorphous oxide films of the barrier type [16].

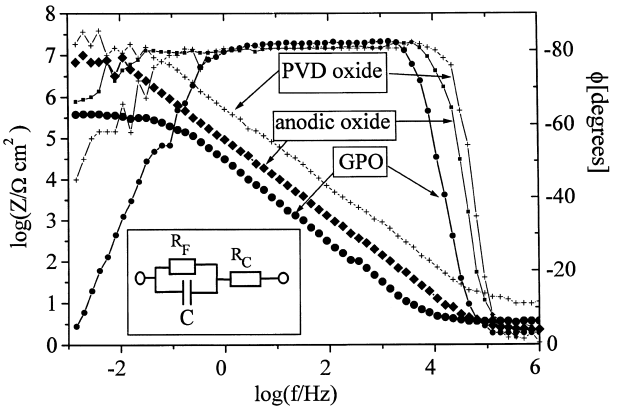

Fig. 2. Impedance spectra of Al/oxide/Ag junctions with differently prepared oxide films: gas phase oxidation (GPO), physical vapour deposition (PVD, 10 nm), and anodic oxidation (10 nm) in aqueous electrolyte.

Parts of the wire specimen were covered by a protective lacquer to avoid breakdown phenomena due to locally enhanced field strength at the tip area (Fig. 1). This coverage ensures also a well defined tunnelling area and enhances the persistence of the electrode against mechanical stress (mounting of the top electrode with the contact wire). To control the preparation process, the anodic oxide film was characterised by electrochemical impedance spectroscopy. Rinsing with Millipore water removes rests of sticking electrolyte.

3.3. Top electrode

3.3.1. Evaporated silver films

The experimental parameters for the evaporation on glass slides are given in Section 2.1. Wires required a special treatment. To ensure a complete coverage it is necessary to rotate the specimen during evaporation. The rotation speed was 1 rps. Since the silver is deposited only in the area facing the source, the film thicknesses determined by the values of the quartz crystal micro balance are larger than the real ones. The silver film thickness was about 50 nm assuming a correction factor of 1/3.

3.3.2. Electrolyte contact

Lots of investigations had been carried out using an Al/Al_2O_3/electrolyte system where the oxide film was formed anodically [8]. Problems caused by polarisation effects at the counter electrode or by a potential drop within the electrolyte due to a current flow were avoided using a three electrode system. To minimise the potential failure the potential of the reference electrode was taken using a Haber–Luggin capillary.

4. Results

The previous mentioned preparation techniques yield a large number of possible layer sequences. We investigated the systems:

- Al film/gas phase oxide/Ag: Section 3.1, Fig. 2; Section 3.3.1, Fig. 6; Section 4, Fig. 8;
- Al film/PVD oxide/Ag: Section 3.1, Fig. 2; Section 3.3.1, Fig. 6; Section 4, Fig. 8;
- Al wire /anodic oxide /Ag: Section 3.1, Fig. 2; Section 3.1, Fig. 4; Section 4, Fig. 8;
- Al wire /anodic oxide/ electrolyte: Section 3.1, Fig. 4; Section 3.2, Fig. 5;
- Al wire/ anodic oxide / electrolyte: Section 3.2, Fig. 5; Section 3.3.2, Fig. 7;
- Al film/gas phase oxide / electrolyte: Section 3.2, Fig. 5; Section 3.3.2, Fig. 7;
- Al film/ PVD oxide / electrolyte: Section 3.3.2, Fig. 7.

4.1. Impedance data

In a first step, differently prepared oxide films were characterised by their impedance. Fig. 2 shows the spectra of the three specimen Al/GPO/Ag, Al/PVD oxide/Ag and Al/

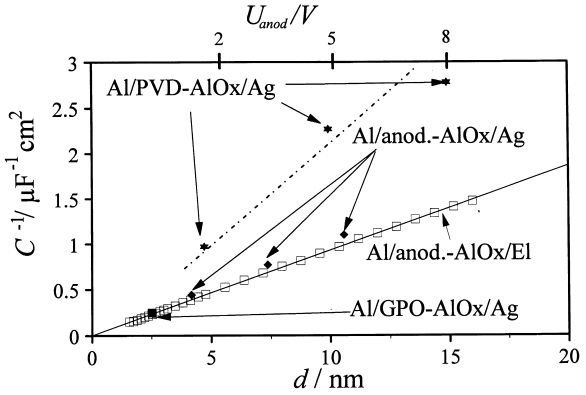

Fig. 3. Reciprocal capacity from impedance spectra as a function of the film thickness d. The corresponding anodisation potential U_{anod} is given for comparisons (formation factor $k = 1.6$ nm/V).

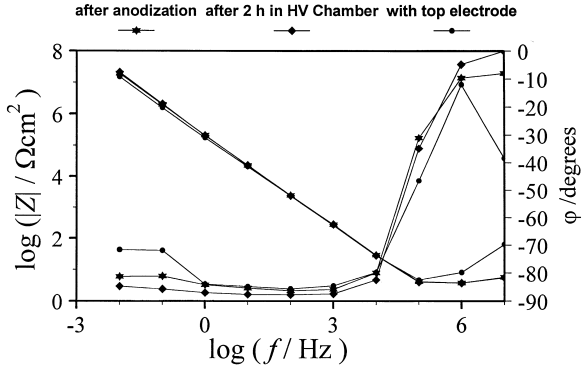

Fig. 4. Impedance spectra of wire type specimen at different stages of preparation: immediately after anodisation (Al/oxide/electrolyte), after 2 h in UHV chamber, and after evaporation of the silver top electrode.

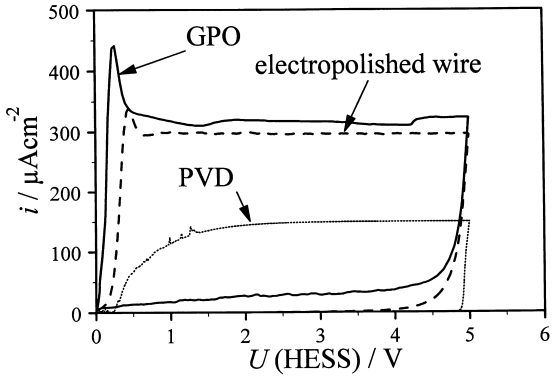

Fig. 5. Cyclovoltammograms of further oxide formation of differently prepared aluminium oxide films (GPO, PVD, electropolished Al wire) in aqueous acetate buffer. Scan rate dU/dt = 100 mV/s.

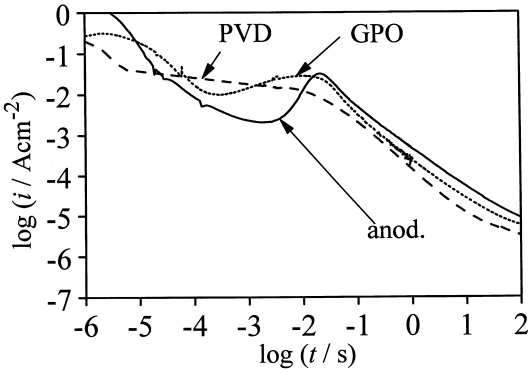

Fig. 7. Current transients of further anodic oxide formation of differently prepared oxide films for different potential steps: from 0 to 7 V for anodic oxide (10.6 nm) on an Al wire, from 0 to 0.5 V for GPO (2.6 nm) on evaporated Al, and from 0 to 5 V for PVD (10 nm) on evaporated Al.

anodic oxide/Ag. The two latter ones have a nominal thickness of 10 nm; for the GPO a thickness of 2.5 nm was assumed (see Section 4.2). The impedance data were fitted (using a non-linear-least-square-fit) by the same simple equivalent circuit, which is given as an insert in Fig. 2, where C is the film capacity, R_f the film resistance and R_c the resistance of the contacts and connectors. Albeit the nominal thicknesses of the PVD oxide and the anodic oxide layer were equal, the spectra differ significantly. A capacity of 1.26 µF/cm^2 for the anodic oxide layer and of 0.34 µF/cm^2 for the PVD layer was yielded.

Fig. 3 shows reciprocal capacity values taken from such impedance spectra versus film thickness. A straight line in Fig. 3 indicates the validity of the simple parallel plate condenser model. The normalised capacity C of a specimen of the area A is given by

$$C = \frac{C'}{A} = \frac{\varepsilon_0 \cdot \varepsilon_r}{d} \quad (1)$$

where ε_r is the relative dielectric permittivity and d is the film thickness.

The Al/anodic-AlO$_x$/Ag specimen shows a linear behaviour according to Eq. (1). The evaluation of the slope yields a dielectric permittivity of $\varepsilon_r = 12$. This value is comparable to those found by other authors [18,20,21]. A very similar value of $\varepsilon_r = 11$ was taken from electrochemical impedance measurements, i.e. in the Al/oxide/electrolyte system [18].

Since the thickness of the GPO layer could not be varied only one data point is listed in Fig. 3. Up to now the thickness of the GPO oxide layer is unknown. From experiments with further anodic oxide growth (see Section 4.3.2) a thickness of 2.5 nm will be taken. This thickness fits perfectly to the data of the anodic oxide films in Fig. 3, i.e. the dielectric properties of anodic and gas phase oxide films seem to be equal.

The thickness $d = 10$ nm of the PVD film was calculated from the frequency changes of the quartz balance in the UHV chamber, assuming a dense oxide film. The capacity of the PVD layer and of the anodic oxide differ for the same thickness, i.e. the relative dielectric permittivity of PVD films, taken from the slope in Fig. 3, is significantly smaller ($\varepsilon_r = 4$) than for anodic films. This mismatch indicates a completely different structure. Obviously PVD films are

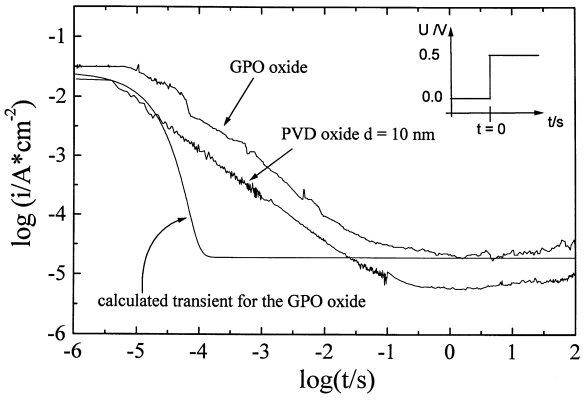

Fig. 6. Current transients of an Al/oxide/Ag junction, potential step from 0 to 0.5 V in double logarithmic presentation; comparison of GPO and PVD and a calculated transient for the GPO oxide film.

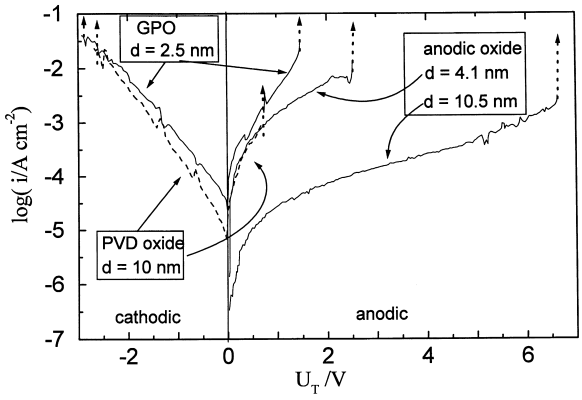

Fig. 8. Tafel plot of MIM contacts with differently prepared aluminium oxide films. The preparation method and the resulting oxide film thicknesses are given as inserts. Breakdown is indicated by an arrow symbol.

much less dense than anodic films. A fraction of pores of about 60% must be assumed.

The small differences of ε_r between the systems Al/anodic-oxide/Ag and the Al/anodic oxide/electrolyte should be due to small deviations of the different specimen. To exclude an artefact of the transfer to the vacuum during evaporation of the silver electrode additional experiments were carried out. Fig. 4 shows impedance spectra of one individual specimen (wire type) at different stages of the preparation. The dashed spectrum in Fig. 4 shows the impedance in electrolyte contact immediately after anodic formation. Then the wire was rinsed with Millipore water and transferred to the UHV chamber and stored for two hours at a pressure of 1×10^{-4} Pa. After this the sample was immersed back into the electrolyte and characterised by a second impedance spectrum. These two spectra coincide almost perfectly, i.e. the transfer to vacuum and back to the electrolyte has no influence on the film properties.

In a next step, after rinsing, the silver top electrode was evaporated in vacuum. The spectrum of the resulting MIM contact in Fig. 4 fits the two others very well. This means the impedance spectra are dominated by the bulk properties of the film; the interfaces oxide/Ag or oxide/electrolyte have only negligible influence. The film properties do not change even though the phase boundary oxide/top electrode changes dramatically. The small differences of MIE and MIM at frequencies >10 kHz are caused by the electrochemical set-up, especially the non-linearity of the reference electrode [22].

Spectra with electrolyte contact were recorded only down to 10^2 Hz to limit the exposure to the electrolyte. In fact, thickness changes due to corrosion are small. In the acetate buffer used here the film thickness decreases by 250 fm/s [17].

4.2. Cyclovoltammetry

So far the microscopic structure of gas phase oxide and anodic oxide seemed to be equal, the PVD were assumed to be porous. Since oxide films on aluminium are stable at potentials U_{form}, the thickness distribution of previously formed oxide can be monitored during further oxide growth. In Fig. 5 the cyclovoltammograms of differently prepared oxide films are shown. The potential was increased by $dU/dt = 100$ mV/s.

During the anodic sweep the current is negligible until the potential comes close to the former oxide formation potential. Then the current increases rapidly and becomes constant (plateau current of further oxide formation). The small current overshoot at end of the rising edge is due to an injection of charge carriers from both boundaries [8]. Due to these kinetic hinderings the oxide growth is delayed and therefore shifted to higher potentials. This shift depends on the scan rate and is about 100 mV at $dU/dt = 100$ mV/s. The start potential of oxide growth was characterised by the point of inflection in the rising edge. An evaluation of the potentiodynamic curves delivers the unknown film thickness using a film formation factor of 1.6 nm/V [17] and a potential of zero thickness of −1.6 V [17].

Accordingly an absolute thickness of 2.6 nm was determined for the GPO layer (Fig. 5). For comparisons the cyclovoltammogram of an electropolished Al wire is shown with a similar thickness of 2.9 nm. This indicates again that evaporated aluminium films and electropolished wires form similar oxide films.

In the case of the PVD films the current increases in a wide potential range from 0.25–3 V. This behaviour is typical for oxide films with a thickness distribution [23]. A precise analysis leads to a film thickness distribution from 3 nm up to 8 nm, i.e. a porous structure. Another remarkable effect is the plateau current which is about two times smaller than for the other oxide films. This indicates a partial blocking of the surface by the special oxide formed during the physical vapour deposition. Pores remain in the oxide and form a sponge structure. Some of these pores within the oxide geometrically block parts of the surface which are not involved into further oxide growth. The porous structure will be also proved by the current transients of potentiostatic pulse experiments (see Section 4.3.2).

4.3. Characterisation by current transients of potentiostatic pulse experiments

The intended use of tunnel junctions requires an identification of all partial currents through the junctions. Normally, the current is assumed to be an electronic tunnel current only and used to calculate the efficiency of hot electron production. Potential step experiments in electrochemical environment show a large number of electronic and ionic conduction mechanisms and allow their separation [24]. Due to the different time laws of each process, following processes were separated in the current transients:

1. Debye-charging of the oxide films (finished after some 10 μs)
2. Dielectric relaxation of the oxide film [25–28] (detectable from 10 μs to 1 s)
3. Electron tunnelling [1] (possible only, if process 1 has completed)
4. Ion migration and high field oxide growth [29] (>100 ms)
5. Corrosion [30] (dominant after some 1000 s)

In addition further information on the thickness distribution of the differently prepared oxide films can be achieved.

4.3.1. Capacitive charging

From the impedance spectrum in Fig. 2 the capacity and the serial contact resistance (resistance of the electrolyte or the silver top electrode) were determined. The serial resis-

tance is about 10 Ω, the capacity depends on the thickness and is in the range of 100 nF/cm^2–4 μF/cm^2. The resulting time constants vary from 1 to 40 μs. Therefore the Debye-charging of the oxide is dominant for some 10 μs only. This means that a time resolution of 1 μs is sufficiently high for these investigations.

Fig. 6 compares current transients of potentiostatic pulse experiments (steps from 0 to 0.5 V) of GPO and PVD specimen with a calculated transient. For the calculation the equivalent circuit from Fig. 2 is used. The periods of Debye-charging ($10^{-6} < t < 10^{-4}$ s) and of constant current ($t > 0.1$ s) are in good agreement with the calculated transient. In between the transients show a linear behaviour in the double logarithmic plot with a slope of $\mathrm{d}(\log i)/\mathrm{d}(\log t) = -1$. This behaviour is typical for dielectric relaxation in oxide films [28] (frequency dependent capacity C) and therefore a dipole effect rather than a charge transport.

This shows that a dominance of tunnel currents can be expected only some ms after the potential step. Our intended source of hot electrons shows an intrinsic time constant due to the relatively large capacity of the thin oxide films.

4.3.2. Potentiostatic oxide formation

Current transients of potentiostatic pulse experiments had been used to enlighten the mechanism of the anodic oxide formation on valve metals. An overview is given in [8]. Fig. 7 compares current transients of potentiostatic pulse experiments during further anodic oxide formation. Again differently prepared specimen were measured in the electrolyte: Al film/gas phase oxide, Al film/PVD oxide and Al wire/anodic oxide.

According to the classification in Section 3.3.1 we divided the anodic transient into the four sections Debye-charging (up to 2×10^{-5} s), Dielectric relaxation (2×10^{-5}–10^{-3} s), Ion migration and high field oxide growth (10^{-3}–10^{2} s) and stationary corrosion ($>10^{2}$ s). An additional tunnelling current was not detected due to the initial oxide thickness in this example (10.5 nm).

The current peak (''overshoot'') is an artefact of anodic oxide formation and is characterised by the time of maximum t_{max} (about 2×10^{-2} s) which is approximated [8] by

$$t_{max} = \frac{\rho d}{i_0 \exp(\beta E)} \tag{2}$$

where ρ is the concentration of mobile ions, i_0 and β are oxide specific constants, and E is the field strength within the oxide. E is calculated from

$$E = \frac{U - U_0}{d} \tag{3}$$

where U_0 is the potential for the thickness $d = 0$.

This means that t_{max} is an extremely sensitive measure (due to the term $\exp(\beta \mathrm{E})$) of the thickness d. Accordingly, well defined homogeneous films yield one sharp peak. Terraced films with areas of different thicknesses yield separated peaks for every thickness [23]. Therefore, the distribution of the oxide thickness can be determined by current transients using Eq. (2).

Two types of problems appear with this analysis. At first the exact determination of the numerical parameters of Eq. (2) is difficult. The potential of zero thickness cannot be obtained experimentally because strong hydrogen evolution and corrosion prevent exact measurements at $U_{Hess} < -1$ V. It must be taken from numerical extrapolations. Therefore, values of the field strength E are somewhat uncertain in electrochemical environments. Best results were obtained using $i_0/\rho = 8 \times 10^{-21}$ cm/s, $\beta = 44$ nm/V, and $U_0 = -1.6$ V [17].

Further problems arise from the structure and properties of the oxide films. Anodic oxide films consist of Al_2O_3 and are free of excess water [8]. They are very stable on wires, anodic oxidation of aluminium films, however, reduces there the adhesion at the interface Al/glass substrate. This may be due to the large current densities in the extremely thin metal film during anodisation. As a result the Al films flake off in the electrolyte after some 100 s. Gas phase oxides on Al films, on the other hand, are stable in the electrolyte. They have very similar properties and, therefore, should have the same compositions as anodic films. The porous PVD oxides might show some swelling effects (uptake of water, transformation from oxide to hydroxide) due to their large surface. Therefore it is necessary for GPO and PVD films to minimise the time of electrolyte contact before starting the current transient. To solve this problem a special immersion machine was used [23], which works with an acceleration of 60 g. This reduces the immersion process to 2 ms. Directly after immersion the transients were recorded.

In the case of the anodic oxide one sharp peak (Fig. 7) is observed. A calculation according to Eq. (2) yields a thickness of 10.4 nm. From the width of the peak a local fluctuation of the oxide thickness of less than ±0.3 nm is estimated [23].

The peak of the GPO indicates a thickness of 2.6 nm. The width of the GPO peak seems is somewhat larger and indicates a larger relative thickness fluctuation (±0.2 nm).

In the transient of the PVD oxide the current maximum is smeared out (Fig. 7). A thickness distribution in the range from 3 to 8 nm was already derived from the cyclovoltammograms. Due to the high sensitivity of the transient experiments according to Eq. (2) only the thickness range from 6.5 nm (10^{-5} s) to 8 nm (10^{-2} s) is observed in the PVD transient. These results are in agreement with the measurements in Section 4.2.

5. MIM Tafel plots

In the previous sections structure and properties of differ-

ently prepared specimen were determined. Now the tunnel characteristics of Al/oxide/Ag will be presented. Fig. 8 shows Tafel plots of such MIM systems. The values were taken from cyclovoltammograms with a scan rate $dU/dt = 100$ mV/s.

For the GPO film the Tafel plot is linear and similar for positive (Al base electrode positive, anodic) and negative tunnel voltages. The curve is not symmetric, the anodic branch is shifted by about 500 mV to cathodic potentials. These tunnel junctions are stable up to 2.2–2.7 V, the breakdown of the specimen is indicated by an arrow. By a breakdown the tunnel junction is destroyed. This is characterised by a sharp increase of current (several decades) and a total loss of capacity. Now the samples behave as Ohmic resistors with a resistance of about 50–100 Ω cm^2. From the breakdown voltages a breakdown field strength of 11–14 MV/cm was calculated. Similar values were reported by Greuel [31] and Tajima [32].

The cathodic branch of the GPO and the PVD specimen are of same magnitude. Therefore the effective tunnel distance of the PVD layer must be in the range of the thickness of the GPO layer (2.5 nm). This proves again the porous structure of the PVD films. Obviously the bottom of the pores is oxidized up to about 2.5 nm by air contact. In addition a sufficient amount of silver enters the pores during evaporation to give a contact. This is true for about 30% of the surface, since the tunnel current is three times smaller than for the GPO sample.

The anodic oxide specimen shows a linear anodic branch with a smaller slope. The thickness dependence of the current is surprising. An increasing thickness from 4.1 to 10.5 nm decreases the current by less then two decades. For a pure electronic tunnel process, however, five decades were expected [11]. This indicates an additional ionic contribution. This is more obvious for the cathodic branch: Cathodically polarised anodic oxide films (Al negative) always show an Ohmic behaviour with resistances of 100–1000 Ω cm^2. This current must be assigned to an ionic conductivity, presumably to protons [19,33] and therefore not shown in Fig. 8. Protons may be incorporated in the oxide or come from an monolayer of hydroxide at the former oxide/electrolyte interface. Such a monolayer of OH may cause asymmetries in Al/anodic oxide/Al systems [34,35].

6. Summary

Tunnel junctions of the type Al/Al oxide/Ag can be used to emit hot electrons of about 2 eV to the environment if the oxide film has a thickness of less than 5 nm and the Ag top electrode of less than 20 nm. The hot electrons can be emitted to an adjacent electrolyte and cause redox reactions [6]. The aim of our work was the development of a production technique of tunnel systems, which are stable at room temperature in atmosphere and in electrolyte.

Two types of Al base electrodes (wires and evaporated films on glass), three types of oxide films (gas phase oxidation, anodic oxidation and physical vapour deposition) (see Fig. 9) were combined with an Ag top electrode film of 15 nm. In addition the oxide film was characterised by measurements in system Al/oxide/electrolyte.

PVD oxide films are porous with a large thickness distribution and two types of pores. One type is wetted by the electrolyte and therefore participates in further anodic oxide growth. A PVD oxide film of nominal 10 nm e.g. (thickness determined by quartz balance) shows wetable pores with net film thicknesses in the range from 3 to 8 nm. Pores of less than 3 nm are not observed, because air contact after removement from the UHV chamber forms a GPO layer at the bottom of the pores. The other type is not wetted and geometrically blocks part of the surface (about 50%) from further oxide growth. The volume fraction of the pores is about 30% and reduces the nominal relative dielectric permittivity to four. The pore structure causes a rough silver top electrode and therefore a weak corrosion resistance. Stable oxide films were only obtained for the pairs Al wire/anodic oxide and Al film/gas phase oxide. The oxides are almost equal in their dielectric properties (relative permittivity $\varepsilon_r = 11.5$–12) and in further anodic oxide growth. The oxides form dense homogeneous films independent of the sample geometry. Even on drawn aluminium wires MIM systems can be built up with oxide thicknesses down to 3 nm. Anodic films can be formed with various thicknesses, but ionic currents may come close to or exceed the tunnel currents, especially if the base electrode is nega-

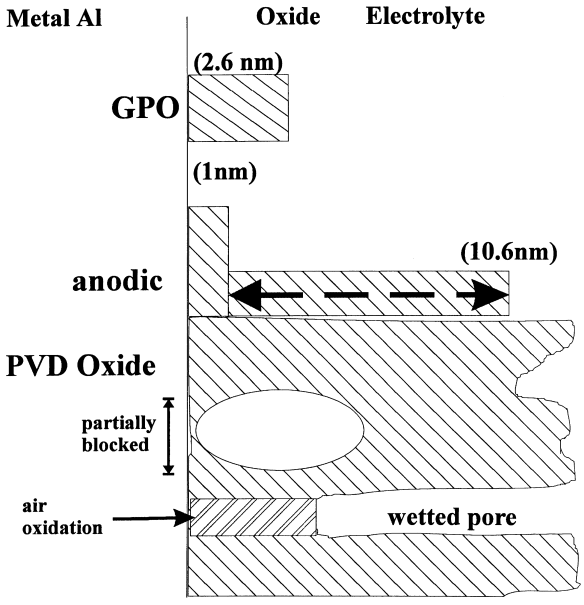

Fig. 9. Scheme of the oxide structures for electrochemical investigations. Gas phase oxides at 298 K are 2.6 nm thick. Anodic oxide films can be varied in a wide range down to 1 nm, in the present paper the thickness is varied up to 10.6 nm. PVD Oxides develop two types of pores, one type is not wetted by the electrolyte and, therefore partially blocks the surface. Uncovered Al can be present at the bottom of wetable pores and are oxidised to about 2.6 nm by air contact during transfer to the electrolyte.

tively polarised. Gas phase oxides behave almost symmetrically for both polarisations, but can not be varied in thickness. Thicker films are obtained at higher temperatures, but crystallisation tendencies must be expected at temperatures higher than 60°C. Accordingly specimen formed at 80°C are usually shortcircuited. Oxide films formed in humid air are less homogeneous in thickness and the band gap decreases from 9 to about 3 eV [16,33].

Altogether the most convenient junction sequence was Al film/gas phase oxide (2.5 nm)/Ag (15 nm). With these junctions an emission efficiency of hot electrons into an adjacent eletrolyte of about 30% (at 1 mA/cm^2) becomes possible.

Acknowledgements

The financial support of the Deutsche Forschungsgemeinschaft and the AGEF e.V. Institut an der Heinrich-Heine-Universität Düsseldorf is gratefully acknowledged.

References

[1] J.G. Simmons, J. Appl. Phys. 34 (1963) 9.
[2] J.J. Quinn, Phys. Rev. 126 (4) (1962) 1453.
[3] D. Pines, D. Bohm, Phys. Rev. 85 (2) (1952) 338.
[4] J. Watanabe, Y. Uehara, J. Murota, S. Ushioda, Jpn. J. Appl. Phys. 32 (1993) 99.
[5] H. Janssen, D. Diesing, A. Otto, Surf. Sci. 331 (1995) 1267.
[6] D. Diesing, H. Janssen, A. Otto, Surf. Sci. 331 (1994) 289.
[7] D. Diesing, S. Rüβe, A. Otto, M.M. Lohrengel, Ber. Bunsenges. Phys. Chem. 99 (1995) 1402.
[8] M.M. Lohrengel, Mater. Sci. Eng. R 11 (1993) 243.
[9] J.W. Diggle, T.C. Downie, C.W. Goulding, Chem. Rev. 69 (1969) 365.
[10] A. Otto, D. Diesing, H. Janssen, et al., in: M.W. Roberts (Ed.), IUPAC, Interfacial Science A, Chemistry for the 21st Century Monograph, 1997, Chapter 7, pp. 163–193.
[11] D. Diesing, Thesis, Heinrich-Heine-Universität, Düsseldorf, 1996.
[12] T. Ismer, Diplomarbeit, Heinrich-Heine-Universität, Düsseldorf, 1994.
[13] S. Rüβe, Thesis, Heinrich-Heine-Universität Düsseldorf, Verlag Shaker, Aachen, ISBN 3,826,509,390, 1995.
[14] J. Gnoinsky, F.K. Crundwell, S.W. Orchard, Mater. Sci. Forum 185 (1995) 667.
[15] E. Clauberg, Diplomarbeit, Heinrich-Heine-Universität, Düsseldorf, 1995.
[16] S. Ono, J.H. Nordlien, E. Akijama, K. Asami, K. Hashimoto, K. Nisancioglu, N. Masoku, 7th Int. Symp. Passivity, Clausthal, 1994.
[17] A.W. Hassel, M.M. Lohrengel, Mater. Sci. Forum 185 (1995) 581.
[18] A.W. Hassel, S. Rüβe, M.M. Lohrengel, J.W. Schultze, Bull. Chem. Technol. Maced. 13 (1994) 49.
[19] H. Takahashi, K. Fujiwara, M. Seo, Corros. Sci. 36 (1994) 689.
[20] D.J. Sharp, J.K.G. Panitz, R.M. Merrill, D.M. Haaland, Thin Solid Films 111 (1984) 227.
[21] M.J. Dignam, in: J.W. Diggle (Ed.), Oxides and Oxide Films, 1, Marcel Dekker, New York, 1973, pp. 92.
[22] A.W. Hassel, Thesis, Heinrich-Heine-Universität, Düsseldorf, Verlag Shaker, Aachen, ISBN 3,826,529,812, 1997.
[23] M.M. Lohrengel, S. Rüβe, Mater. Sci. Forum 185 (1995) 611.
[24] M.M. Lohrengel, Ber. Bunsenges. Phys. Chem. 97 (1993) 440.
[25] H. Kliem, G. Arlt, Solid State Comm. 59 (1986) 793.
[26] H. Kliem, IEEE Trans, Electr. Insul. 24 (1989) 185.
[27] A. K. Jonscher, Dielectric Relaxation of Solids, Chelsea Dielectrics Press, London, 1983.
[28] S. Rüβe, M.M. Lohrengel, J.W. Schultze, Solid State Ionics 72 (1994) 29.
[29] A. Güntherschultze, H. Betz, Z. Phys. 68 (1931) 145.
[30] M.M. Lohrengel, Electrochim. Acta 39 (1994) 1265.
[31] G. Greuel, Thesis, Rheinisch-Westfälische Technische Hochschule, Aachen, 1994.
[32] S. Tajima, Electrochim. Acta 22 (1977) 995.
[33] T.D. Burleigh, 7th Int, Symp. Passivity, Clausthal, , Abstracts, p. (1994) 58.
[34] A.W. Hassel, M.M. Lohrengel, Electrochim. Acta 40 (1995) 433.
[35] H. Sambe, D.E. Ramaker, J. Vac. Sci. Technol. A 10 (1992) 2991.